Article:
Kattikat Melcom, D. T., Tsekhanovich, I., Guezet, F. et al. (2026) Fission mode identification in the 180Hg region: Derivative analysis approach. Physical Review C. 014627. ISSN: 2469-9993

https://doi.org/10.1103/qx28-3tkb

Fission mode identification in the ^{180}Hg region: derivative analysis approach

K. M. Deby Treasa,* I. Tsekhanovich, and F. Guezet

University of Bordeaux, CNRS, LP2I Bordeaux, UMR 5797, Gradignan, F-33170, France

A. Andreyev

Department of Physics, University of York, York YO10 5DD, UK

K. Nishio

Advanced Science Research Center, JAEA, Tokai, Ibaraki 319-1195, Japan

Background: Experimental setups commonly used to study fission properties of nuclei in the exotic neutron-deficient ^{180}Hg region are based on the time-of-flight technique for the fission-product identification. In best cases, the obtained fragments mass (FFMD) and total kinetic energy (TKE) resolution does not exceed 2 u and 6 MeV, respectively. In addition, the nuclei of interest are created via fusion reactions and at excitation energies of several tens of MeV. The deduced final fission-fragment mass distributions are therefore in general structureless, which makes the identification of fission modes, and their weight determination, ambiguous and author-dependent.

Purpose: To develop a robust analysis approach aiming at identification of number of major fission modes in the fission-fragment mass distributions from fusion-fission reactions.

Method: We use the GEF code to simulate the FFMD - TKE data for a classical actinide nucleus (^{240}Pu) considered at different excitation energies, as well as we construct FFMDs with different compositions for a hypothetical A=180 nucleus. The influence of the excitation energy and of the experimental mass resolution are investigated by the ability of the direct FFMD and FFMD-TKE fit to reproduce the input data parameters. The 1^{st} and the 2^{nd} derivatives calculated from the simulated and resolution-affected FFMD data are analysed in terms of the presence of extrema and inspected with respect to the initial data reproduction when fitted with the appropriate fit functions.

Results: The resolution effect is found to broaden the simulated FFMD and TKE data, as well as to smear structures in the 1^{st} and 2^{nd} derivatives thus limiting the sensitivity of the method to a few per-cent level in the fission-mode weight. Direct fit of the resolution-affected FFMD and FFMD-TKE data is found to be unable to find the asymmetric-mode positions nor to reproduce the modes weights in both ^{240}Pu and A=180 nuclei, especially if the used fit-function composition does not correspond to the input data. The fission-modes characteristic TKE values are also not reproduced in a non-constrained fit. *In contrario*, the simulated data could be safely reproduced with fit functions constructed with help of the 2^{nd} derivative curves, the detected minima being the signature of number of fission modes detectable in the resolution-affected data. The power of the used method is demonstrated with a set of fusion-fission data for the ^{180}Hg nucleus.

Conclusions: The derivative analysis if applied to the simulated limited-resolution data appears to provide consistent results on the fission-mode parameters, such as positions and widths, even for the cases of strong dominance by the symmetric mode, i.e. for Gaussian-like FFMD shapes. The method is shown to work also on data sets with limited statistics (real experimental data with integral of a few tens of thousands of events); the use of several derivative-window lengths is strongly recommended for more reliable identification of the number of extrema and their positions.

INTRODUCTION

The process of nuclear fission, i.e. the splitting of a single nucleus into several fragments, remains one of the least comprehended fundamental phenomena in nuclear physics. Although the macroscopic Liquid Drop Model (LDM) could quantitatively explain the phenomenon of fission straight after its discovery in 1938 [1], its full understanding is yet to be achieved. The historical observation of unequal mass split in ^{236}U, known today as the asymmetric-fission mode (A mode), has been confirmed in various experiments with different actinide nuclei [1]. This A mode produces a double-humped fission-fragment mass distribution (FFMD) and is understood to be driven by the nucleon pairing and shell effects. The latest theoretical works refer to the octupole deformation of fragments with atomic numbers $Z = 52$ and 56 [2, 3] as responsible for the major mass-asymmetric splits in fission of actinide nuclei. In contrast, the symmetric-fission mode (S mode) produces fragments with comparable masses and thus the relevant FFMD exhibits a Gaussian-like shape. The other global difference between the A and S modes is the characteristic values of the total kinetic energy (TKE) of fission products known to be lower for the S mode than for the A-mode. This difference is understood as the consequence of more elongated fission configuration at scission point.

Actinide nuclei are known to exhibit both modes, with their relative contributions to the FFMDs governed by the excitation energy (E^*) [4]. The dominance of the S mode in the FFMDs from fission of nuclei with A<226 established experimentally in the sub-lead region, cf. [5],

* debytreasakm@gmail.com

gave the reason to interpolate the same S-mode dominance also to the sub-lead region. However, the double-humped FFMD obtained in a β-delayed fission (βDF) of very neutron-deficient ^{180}Hg (E^*<10 MeV) had strongly challenged this expectation [6]. From a series of subsequently conducted experiments and theory works, it is now firmly established that the mass-asymmetric fission is not a property unique to ^{180}Hg but is relevant to a wide range of nuclei around it, cf. Refs. [7–23].

Unlike the actinide region, nuclei in the vicinity of ^{180}Hg are short-lived and can be produced in quantities sufficient for fission studies nearly exclusively by fusion technique. Here, the low mass asymmetry between fission fragments ($\sim$20 u, contrary to $\sim$40 u in actinides, cf. [6]), along with a non-perfect fission-fragment mass identification and high E^* of fissioning nuclei inherent in fusion-fission reactions, introduce serious difficulties in the FFMD content determination.

In the sub-lead region, the identification of fission modes, along with the determination of their relative weight in the measured data, is typically reliant on the fit function employed to reproduce experimental FFMD and TKE distributions. This makes the obtained results highly author dependent: absence of any known prominent structures in the relevant data makes the choice of the used fit function composition debatable. For instance, in Refs. [7, 9, 16], the FFMDs were described with a sum of 2-Gaussian (2G) functions centred at complementary fragment masses, and the symmetric-fission mode was not considered. Two fission-mode analysis (3G fit) of FFMDs was used, i.e., for ^{178}Pt [11, 13] and Bi isotopes [24], whereas a 5G and/or 7G fit was implemented for analysis of the FFMDs from fission of ^{180,182,183}Hg, ^{178}Pt, and ^{182,192}Pb [8, 12]. The 5G description of the data was recently extended to two dimensions, which allowed for simultaneous fitting of the mass-TKE matrix [18]. In the cited cases, the authors rely on the obtained χ^2 value to justify the composition of the used fit function. However, the quality of data description comes inline with the complexity of the used fit function, the latter having no obvious link to the underlying physics. In addition, none of the works published so far accounts for the impact of the non-perfect experimental resolution on the obtained results.

This paper addresses the outlined problem of the fission-mode identification in the FFMD and TKE data from fission of nuclei from the pre-lead region. We use a set of simulated data to show the effect of limited mass resolution on the capability of the fission-mode detection and identification of their properties made with help of a classical functional-analysis approach based on the second derivative behaviour. The applicability limits of the used method are indicated. Its power is demonstrated with a set of fusion-fission data for the ^{180}Hg nucleus taken from [7].

FFMD AND TKE DATA ANALYSIS METHODOLOGY

In order to understand the impact of non-perfect mass and energy resolution on the determination of the FFMD and TKE data composition, a set of data with *a priori* known composition is required. Such data can be simulated with the desired content in terms of the fission modes number and properties (position, width and amplitude).

The simulated one- and two-dimensional data (FFMD and mass-TKE distributions, respectively) are convoluted with experimental resolution values of 2 and 4 u for the mass and 6 and 8 MeV for the TKE, which are the values most frequently cited in the fusion-fission papers in the region around ^{180}Hg.

As a next step, the 1^{st} and 2^{nd} derivatives are calculated from the simulated data sets. The derivative data are then analysed with a set of Gaussian functions $f_i(A)$ describing individual FFMD components as indicated in the following equation :

$$\begin{gathered}
FFMD = \sum_i f_i(A) = \sum_i B_i \exp\left[-\frac{(A-\overline{A_i})^2}{2\sigma^2_{A_i}}\right] \\
f^{'}(A) = FFMD^{'} = \sum_i f_i(A)\frac{\overline{A_i}-A}{\sigma^2_{A_i}} \\
f^{''}(A) = FFMD^{''} = \sum_i \frac{f_i(A)}{\sigma^2_{A_i}}\left[\left(\frac{A-\overline{A_i}}{\sigma_{A_i}}\right)^2 - 1\right]
\end{gathered} \tag{1}$$

Here, the functions $f^{'}(A)$ and $f^{''}(A)$ are composed of i components relevant to each peak in the corresponding fission mode, with B_i, σ_{A_i} and $\overline{A_i}$ being the mode amplitude, width and peak position in the FFMD, respectively. The number of Gaussians to use is given by the number i of minima identified in the 2^{nd} derivative data. For example, i=5 would signify five components in the FFMD, one for the S-mode, two for the first A-mode ($A1$) and further two for the second A-mode ($A2$). The term $f_i(A)$ describing the S- and A-mode components in the FFMD is present in all the three expressions of eq.1. This means that, once the composition of the fit function is determined, the FFMD composition can be obtained from the fit made on any data set (FFMD, 1^{st} or 2^{nd} derivative).

However, it appears that the use of Eq.1 with completely uncorrelated and unconstrained parameters may provide good overall data description in terms of χ^2 but gives meaningless results for fission modes: the S-mode position may appear anywhere in the FFMD or non-identical integral area obtained for the same A-mode components. Therefore, it is recommended to fix the S-mode position at $\frac{A_{CN}}{2}$ and to demand identical widths, amplitudes as well as displacement from the S-mode position for the same A-mode components.

The derivative approach cannot be directly applied to the correlated mass-TKE data. These data are analysed with a set of two-dimensional Gaussian functions, with the number of components i equal to the number of minima found in the second-derivative analysis of the FFMD:

$$f(A,TKE) = \sum_i B_i \exp\left[-\frac{(A-\overline{A_i})^2}{2\sigma^2_{A_i}} - \frac{(TKE-\overline{TKE_i})^2}{2\sigma^2_{TKE_i}}\right] \quad (2)$$

The feasibility of the proposed method for extracting fission modes is tested with two nuclei with a *a priori* known FFMD composition: **i)** ^{240}Pu, for which, in addition to the FFMD, the correlated mass-TKE data set can be obtained at various excitation energies using the GEF code [25], and **ii)** a hypothetical light nucleus with a A=180 u whose FFMD is created by combining different number of fission modes, each with different weight. Finally, the second derivative method is applied for analysis of real data from fusion-fission of ^{180}Hg [7].

RESULTS

Simulated data: ^{240}Pu. The FFMD of a nucleus in the classical actinide region can be best described by using one S-fission and three A-fission modes; here, they are denoted using the Brosa nomenclature [26] as SL and $S1$-$S3$, correspondingly. Each mode is characterised by its position in the FFMD relevant to its origin, by its specific characteristic average TKE ($\overline{TKE}$) relevant to the scission configuration, and by its relative weight W indicating the mode importance in the considered FFMD.

Fig. 1 shows the impact of the limited resolution on the simulated FFMD and mass-TKE. Its major effect is a significant broadening of the FFMD and TKE distributions, which fills in the symmetry and lowers the peak-to-valley ratio.

A sliding window on the FFMDs data is used to obtain the 1^{st} and the 2^{nd} derivative data sets, cf. middle column of Fig. 1 for the resolution effect on the 2^{nd} derivative results. Presence of 7 minima is clearly seen in the initial data set. This number determines composition of the fit function in Eq.1 and implies presence of one S-mode and of three A-modes in the considered FFMD, in accordance with the input data.

From the one- (1D) and two-dimensional (2D) fitting made with the 7G fit function on the simulated and resolution affected data, the corresponding weights W of the S- and A-modes are obtained and can further be compared with the input data. Table I demonstrates this sort of comparison, for a set of excitation energies and for several important fit parameters and results. The following can be stated:

- For the range of considered E^*, direct FFMD fit does not reproduce the modes positions nor their weights, the disagreement with input data being stronger for the resolution-affected data. The major striking feature here is the suppression of the SL-mode, in favour of the $S1$-mode.
- In general, free fit on the 2^{nd} derivative correctly reproduces the major mode positions and weights, despite the non-perfect mass resolution.
- Positions of minor fission modes are less satisfactory reproduced in the 2^{nd} derivative analysis, as seen on example of $S3$, for which the depth of the minima (at A=88/152 u, W=6% at E^*=10 MeV) is strongly affected by the decreasing resolution, cf. middle panel of Fig. 1. With the increasing E^*, the $S3$-mode weight drops below 1% which makes it be hardly detectable even at perfect resolution.
- The 2D free fit fails to reproduce the $\overline{TKE}$ and W data for both S and A modes. Using the 2^{nd} derivative minima to fix the modes positions in the 2D fit function (results not shown in Table I) helps in the $\overline{TKE}$ determination but does not deliver correct W values.

It is worth noting that the simulated data exhibit high statistical precision ($> 10^5$), allowing for determination of W with uncertainty below 1%. We also stress that both the 1D and 2D fits are sensitive to the specified fit boundaries, as also emphasized in Ref. [18]. The associated uncertainty can be gauged by varying the boundary conditions, revealing the value surpassing the statistical one by a factor of 4. Consequently, an overall uncertainty of approximately 4% can be assigned to the 1D and 2D W values in Table I.

Simulated data: A=180. The FFMD of this hypothetical nucleus can be simulated by assuming different S and A mode combinations. In the simulation, we focus on the two selected combinations: one S plus one A mode and one S plus two A modes, the A modes displaced by 10 and 24 u with respect to the centroid $\frac{A_{CN}}{2} = 90$.

The simulated data address the FFMD shapes commonly observed in fusion-fission reactions in the sub-lead region; the input data on fission modes are summarized in Table II. The point of interest here is to make analysis of the resolution-affected FFMD displayed in Fig.2 along with the individual mode components. The 1^{st} and 2^{nd} derivative data obtained from the initial and resolution-affected FFMDs are shown in the columns 2 and 3 of Fig.2, respectively.

As in case of ^{240}Pu, the resolution effect manifests as a flattening of structural features in the FFMD and its derivative data sets. The right column of Fig.2 demonstrates the power of the 2^{nd} derivative analysis: it appears possible to identify the presence of A modes in the non-structured FFMDs with single-Gaussian-like shapes, cf. panels (f,l). In these extreme cases, the presence of the $A1$ mode is evidenced either by a shallow minimum at the $\frac{A_{CN}}{2}$ or by a kink in the slopes, if compared to the pure S-mode derivative from panel (o). The $A1$ mode position can in this case be obtained from the fit of the 2^{nd} derivative data, whereas for more structured FFMDs (panel (c)) it can be read by eye. Panels (j,k,l) illustrate the sensibility of the method to detect the $A2$ contribution to the FFMD, which is kept here on the detection

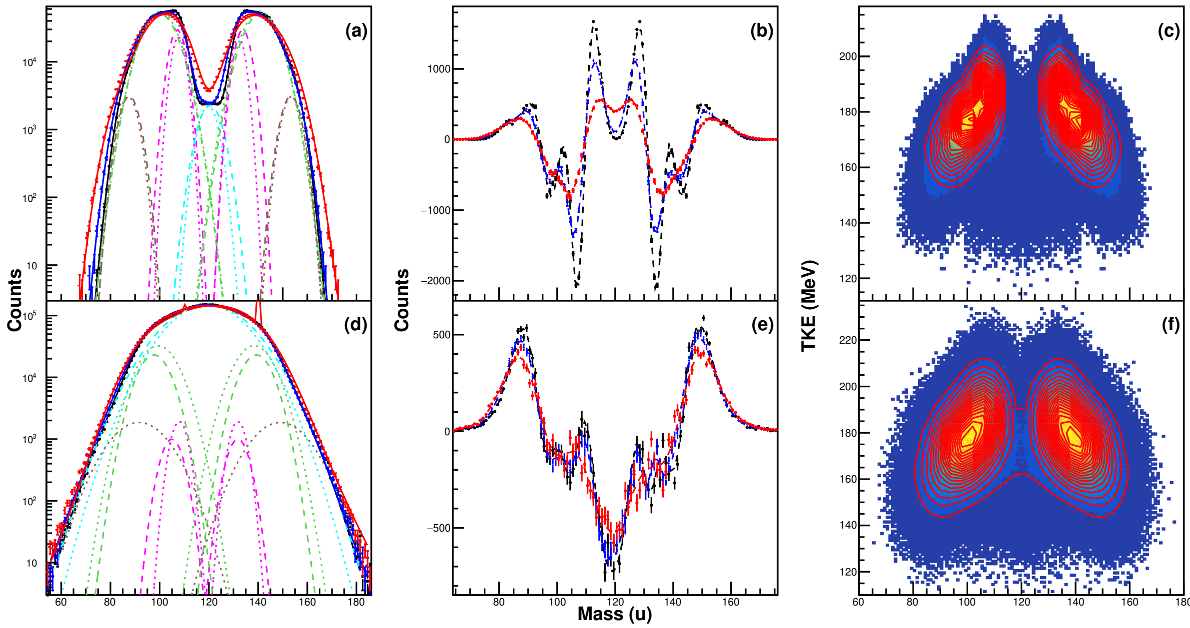

FIG. 1. FFMDs (left column) and their 2^{nd} derivatives (middle column) for ^{240}Pu at two different excitation energies: $E^* = 10$ MeV (upper raw), and $E^* = 50$ MeV (lower raw). Black, blue and red lines depict, correspondingly, the simulated and the 2u- and 4u-resolution affected data sets. The FFMD components are relevant to the fit of the simulated data set (red line) made with free (dotted lines) or constrained (dashed lines) fit function parameters. SL/S1/S2/S3 mode is shown in blue/magenta/green/brown. The right column displays the mass-TKE matrices for $E^* = 10$ MeV : simulated (c) and resolution-broadened data ((f), resolution 4 u for mass and 6 MeV for TKE). Here, red contour lines represent the resultant 2D fit with function from Eq.2.

limit. The minimum visible at A∼66 in panel (l) is expected to become flatter or be completely blurred if the data are measured with resolution worse than 2 u, similar to the $S3$ mode in Fig.1(b). Finally, the presence of the $A1$-mode in the FFMDs with the complete S-mode dominance (90% or higher, cf. panel (g)) cannot be identified from the resolution-affected data, as shown in panel (i).

The 3G and 5G fit functions were used to fit the resolution-affected FFMDs from Table II, along with their 1^{st} and 2^{nd} derivatives. For each fit, the S mode position was kept fixed at 90 u, whereas the A modes parameters were kept free but identical for each particular A mode. Table II compares the obtained results with the input data.

- Similar to the ^{240}Pu case, free direct FFMD fitting is found unable to reproduce the resolution-affected data (modes positions and weights), the agreement being however better for the less complex FFMD composition (S+$A1$ or 3G).
- Second derivative fit is found generally able to identify the composition of the resolution-affected FFMDs. The mode positions correspond to the minima location on the mass axis, their values can be safely obtained from the corresponding fit function. This works even is the case of FFMDs strongly dominated by the S mode, cf. Fig.2(i,l).
- Globally, the 1^{st} derivative fit results are found to deliver similar results for the modes parameters and weights, as the 2^{nd} derivative fit.

Real data: ^{180}Hg. This part demonstrates the use of the derivative approach for the analysis of real data from the study [7] which was the first one, after the asymmetric fission discovery of ^{180}Hg at ISOLDE [6], to use fusion-fission reactions for fission studies in the ^{180}Hg region. It is stated in [7] that the resulting FFMDs "*could be well reproduced with a single asymmetric fission mode*".

Fig.3 shows the ^{180}Hg FFMD data (right column) from [7] analysed for minima in the 2^{nd} derivative curves (left column) for the cases with best statistics (E^*=33.4 - 47.8 MeV). The FFMDs have then been fitted with the 3G fit function whose composition was determined from the identified minima in the 2^{nd} derivative data. The fits were done with both free and fixed position of the A mode, cf. Table III for the results. In general, inspection of the the data and the fit results presented in Fig.3 allows for the following observations and conclusions to be made:

- True experimental FFMDs are limited in statistics and show scattering of data around a smooth shape. This scattering affects the 2^{nd} derivative curve but can be minimised with the choice of the derivative window length, cf. panels (b,d), (f,h) and (j,l).
- Two dip minima are found to be present at all E^* energies, their positions do not change with E^* and

TABLE I. ^{240}Pu : Fission-mode characteristics (weight W, light-fragment peak position A_L and average total kinetic energy $\overline{TKE}$) as given by GEF at different excitation energies E^* and as found in the FFMD (1D), FFMD-TKE (2D) and the 2^{nd}-derivative analysis of the initial (n/ R) and resolution-corrected data (w/ R, experimental mass and energy resolution 2 u and 6 MeV, respectively). χ^2 is the data description quality. The units are % for W, u for A_L and MeV for E^* and $\overline{TKE}$.

E^*	Mode	Input data			n/ R			w/ R									
					1D			1D			Second derivative			2D			
		W	A_L	$\overline{TKE}$	W	A_L	χ^2	W	A_L	χ^2	W	A_L	χ^2	W	A_L	$\overline{TKE}$	χ^2
10	SL	3.0	120.0	165(4)	1.3	120.5	5.74	1.1	120.0	1.12	1.7	119.6	1.77	2.5	119.9	155.0	13.8
	$S1$	20.2	106.9	189(4)	22.0	107.2		21.0	106.7		22.3	106.6		52.1	104.8	184.7	
	$S2$	69.8	99.6	177(4)	73.5	99.8		75.0	99.4		73.0	99.0		1.8	110.0	167.0	
	$S3$	6.0	88.8	162(5)	3.1	88.0		2.8	87.4		2.9	87.4		43.6	95.9	170.0	
30	SL	64.8	119.7	171(6)	95.6	120.5	1.53	81.5	120.0	0.98	75(14)	119.7	1.33	27.2	120.1	163.1	0.93
	$S1$	3.7	106.9	189(4)	0.3	115.5		5.4	116.5		2.4(24)	104.0		55.6	113.3	179.1	
	$S2$	30.4	99.2	178(3)	3.7	101.3		11.5	104.4		12.5(35)	100.0		7.3	90.2	165.0	
	$S3$	1.1	87.9	163(3)	0.4	90.6		1.6	96.5		9.6(29)	80.8		9.9	99.6	170.0	
50	SL	85.4	118.8	173(3)	23.2	119.3	7.18	19.5	118.8	5.27	83.6(23)	118.8	1.39	41.3	119.6	172.9	1.59
	$S1$	1.1	105.7	189(3)	63.8	112.2		66.3	112.6		0.5(2)	105.2		19.4	110.7	183.7	
	$S2$	13.2	98.3	179(5)	13.0	99.1		13.8	99.4		15.2(9)	98.1		29.1	102.7	170.6	
	$S3$	0.3	87.4	164(3)	0.01	91.1		0.3	93.8		0.8(3)	92.0		10.3	99.4	157.4	
70	SL	92.9	117.9	174(4)	21.5	118.4	3.30	15.9	117.9	2.20	94.0(33)	118.2	1.63	0.1	118.4	166.6	1.16
	$S1$	0.6	104.8	190(3)	74.0	111.3		79.2	109.3		0.3(1)	104.7		81.5	110.0	175.8	
	$S2$	6.4	97.3	180(3)	4.4	97.1		3.6	96.6		4.4(5)	97.0		10.6	95.6	173.6	
	$S3$	0.1	86.3	164(3)	0.02	90.0		1.3	79.3		1.3(23)	81.0		7.8	92.0	159.8	

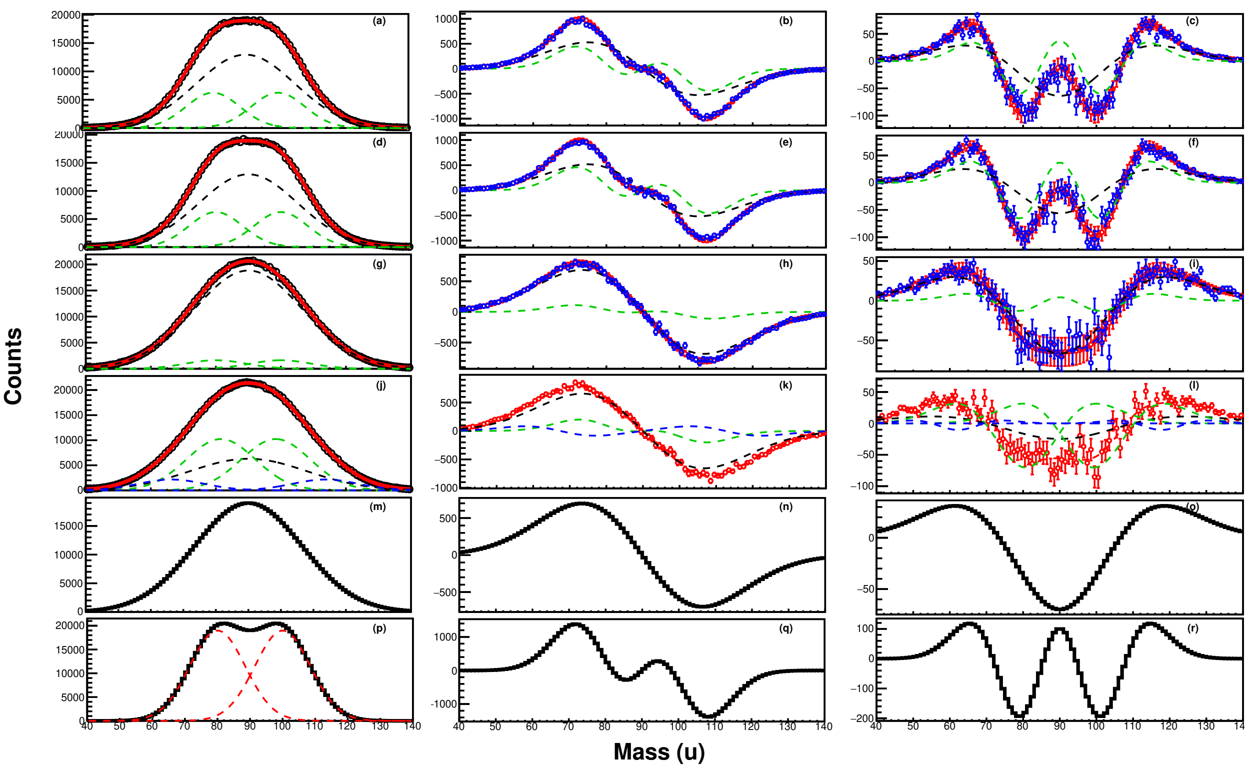

FIG. 2. **Four first rows**: simulated FFMDs (black symbols, left column) affected by the resolution of 2 u and their 1^{st} (middle column) and 2^{nd} (right column) derivatives for different combinations of S and A modes, refer to Table II for input data. Panels (a), (d) and (g): result of the a 3-Gaussian function FFMD fit (red line) fit, the fission modes components shown by black and green broken lines for the S and A modes, respectively. The resting panels demonstrate the resolution effect on the 1^{st} and the 2^{nd} derivative data: blue/red symbols stand, correspondingly, for the initial/resolution-affected data sets. Broken black, green and blue lines in panel (c) are respectively the S, $A1$ and $A2$ mode components from the free parameter fit. **Two bottom rows**: pure S and pure A mode FFMDs and their 1st and 2nd derivatives.

TABLE II. $A = 180$: Direct FFMD and derivative analysis, FFMDs simulated with different contributions from 2 or 3 fission modes and convoluted with 2 u of resolution. S, $A1$ and $A2$ are the symmetric and two asymmetric modes, W (in %) denoting their weight. A_L and σ, in units of u, refer to the light-fragment position and width of fission modes.

Mode	Input data			Fit function: 3 Gauss				Fit function: 5 Gauss			
				FFMD/first/second derivative fit results				FFMD fit results			
	W	A_L	σ^b	W	A_L	σ	χ^2	W	A_L	σ	χ^2
S	65.2	90	15	66/67/73	90	15.1/15.1/15.1	1.03/0.88/1.20	68.8	90	14.9	0.90
$A1$	34.8	80	8	34/33/27	80.0/80.0/80.0	8.2 /8.3 /8.1		30.8	79.8	8.1	
$A2$	—	—	—					0.4	68.3	12.7	
S	82.9	90	16	66/66/66	90	15.1/15.2/15.2	0.86/0.72/1.02	65.3	90	15.6	0.89
$A1$	17.1	80	8.5	34/34/34	80.0/80.0/80.0	8.2 /8.3 /8.3		26.6	80.7	9.2	
$A2$	—	—	—					8.1	72.0	13.3	
S	91.4	90	16.5	91/91/92	90	16.6/16.7/16.8	0.85/0.84/1.34	59.4	90	14.8	0.91
$A1$	8.6	80	9	9 /9 /8	80.0/80.0/80.0	9.2 /9.2 /9.1		34.8	79.4	11.3	
$A2$	—	—	—					5.8	61.7	11.5	
S	84.0	90	16.5	68/66/66	90	16.7/16.9/18.1	1.1/0.96/1.42	30.4	90	18.0	0.80
$A1$	11.4	80	8.5	32/34/34	78.7/79.1/80.1	12.8/12.7/12		57.9	81.6	10.5	
$A2$	4.6	66	8.5	—	—	—		11.7	66.3	10.1	

[b] Accounts for experimental resolution of 2 u

TABLE III. ^{180}Hg: Fission-mode weight W (%), position A_L (u) and width σ (u) from the FFMD fit with a 3-Gaussian fit function with free and constrained A-mode peak positions. χ^2 is the corresponding fit quality. E^* data from [7].

E^*	M	Free A_L position				Fixed A_L position			
		W	A_L	σ	χ^2	W	A_L	σ	χ^2
33.4	S	10(7)	90.0	19(2)	1.59	42(3)	90.0	15.4(1)	1.64
	$A1$	90(8)	78.9(1)	9.3(2)		58(3)	78.0	8.5(1)	
39.8	S	83(4)	90.0	14.7(2)	0.88	52(6)	90.0	15.6(3)	1.15
	$A1$	17(2)	73.8(5)	5.1(5)		48(6)	78.0	8.3(3)	
47.8	S	77(4)	90.0	16.2(1)	4.23	51(3)	90.0	17.0(1)	4.79
	$A1$	23(2)	75.8(4)	7.7(3)		49(3)	78.0	9.4(1)	

can be read directly from panels (b,d) and (j,l). Presence of the S mode in the FFMDs is evidenced by the minimum at A=90 for E^*=33.4 and 47.8 MeV, it can be guessed for E^*=39.8 MeV, by making comparison with shapes (o,r) of Fig.2. With no other minima to be clearly present, the fit function of eq.1 should then be composed of three Gaussians.

- The FFMD data fit with free A-mode parameters shows an irregular drift of the mode position, as well as irregular change in width, with E^*, cf. Table III for numerical values, in contrast to the 2^{nd} derivative data (cf. panels (b,d) and (j,l)).

- FFMD fit with fixed A-mode positions does not lead to the loss of accuracy in the data description, cf. reduced χ^2 values in Table III. The obtained A- and S-mode weights show a small gradual change with E^* which seems reasonable taken into account the change of less than 10 MeV in the effective excitation energy of the nucleus [7].

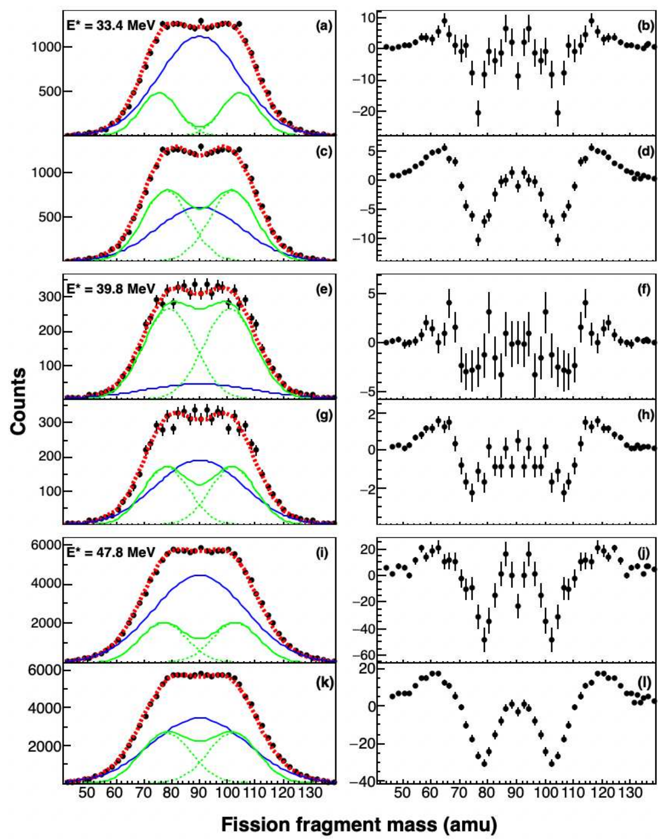

FIG. 3. ^{180}**Hg**: Experimental FFMDs for three beam energies from [7] and their derivatives calculated with window length of 3 u (panels (**b**, **f**, **j**)) and 5 u (panels (**d**, **h**, **l**)). Panels (**a**, **e**, **i**) and (**c**, **g**, **k**) display, respectively, the individual mode components obtained from the FFMD fit with free and fixed A-mode peak positions. Blue/green lines indicate the S/A-mode components, red line describes the FFMD in total. The mass resolution was 2.4 u [7].

CONCLUSIONS

The problem has been addressed of the fission-mode identification in the FFMD ans TKE data obtained in experiments with resolution on the level of several u and MeV, respectively. The resolution effect has been investigated, as a function of excitation energy, on example of two nuclei with extreme properties: a typical actinide nucleus with a well-structured FFMD (^{240}Pu) and a hypothetical A=180 nucleus with a single-Gaussian-like FFMD shape. In general, the resolution effect smears the structures and broadens the FFMD and TKE data thus making fission modes with contribution on a few percent level difficult to detect.

It has been shown that the free FFMD fit is unable to correctly reproduce the input data on the mode positions and weights. More precisely, the A modes are found to shift from their true positions, the shift found to correlate with the mode weight and nucleus excitation energy (larger for higher excitation energies and for minor A modes). The wrong mode position determination leads to an underestimated contribution of the S mode, on expense of the closes $A1$ mode. In addition, the 2D fit of the FFMD-TKE matrix is found to fail in the determination of $\overline{TKE}$ of fission modes, the disagreement can be as large as 10 MeV even for dominant fission modes. This failure can be explained by the presence of multitude of local minima on the mass-TKE surface, whereas the shift of the mode positions is likely to assign to the fit algorithm aimed at the best data description.

Moreover, the FFMD analysis of hypothetical A=180 nucleus affected by 2 u resolution and tested for the direct fit with 3G and 5G fit functions makes it evident that not knowing *a priori* the fit function composition may lead to a wrong physics result: increase of the A-mode contribution with increasing excitation energy. This finding stresses on the importance of having measurements done at several excitation energies.

Simple counting of number of extrema in the 2^{nd} derivative data is shown to be able to resolve the ambiguity in the determination of the FFMD fit function composition. The fit function determined this way can be used directly on the 1^{nd} and/or 2^{nd} derivative data, in order to obtain the fission-modes parameters (positions, amplitude and width) and, consequently, the fission-mode weight. Note that the best precision on the fit parameters is achieved if the fit function is used (or re-used, if the exact mode positions are required) directly with the FFMD data. If applied to a real experimental data set (^{180}Hg from Ref. [7]), the 2^{nd} derivative shows itself capable of detecting — in a simple and undoubted way — the presence of both S and A modes in the FFMD data, even in the case of modest statistics (on the level of a few thousands of events, cf. E^*=39.8 MeV in Fig.3). The A-mode weight obtained for the ^{180}Hg FFMDs with the fixed A-mode position follows expectations for the growing excitation energy, contrary to the free-parameter fit, which adds to the credibility of the used analysis technique.

ACKNOWLEDGMENTS

The authors (K.M.D.T. and K.N.) acknowledge support from French Ministry for higher Education, Research and Innovation (MESRI) and the Bordeaux University.

[1] L. Meitner, O. R. Frisch, Disintegration of uranium by neutrons: a new type of nuclear reaction, Nature 143 (3615) (1939) 239–240. doi:10.1038/143239a0. URL https://doi.org/10.1038/143239a0

[2] G. Scamps, C. Simenel, Impact of pear-shaped fission fragments on mass-asymmetric fission in actinides, Nature 564 (7736) (2018) 382–385. doi:10.1038/s41586-018-0780-0. URL https://doi.org/10.1038/s41586-018-0780-0

[3] G. Scamps, C. Simenel, Effect of shell structure on the fission of sub-lead nuclei, Phys. Rev. C 100 (2019) 041602. doi:10.1103/PhysRevC.100.041602. URL https://link.aps.org/doi/10.1103/PhysRevC.100.041602

[4] E. Konecky, H. Specht, J. Weber, Symmetric and asymmetric fission of Ac isotopes near the fission threshold, Phys. Lett. B 45 (4) (1973) 329–331. doi:https://doi.org/10.1016/0370-2693(73)90047-6. URL https://www.sciencedirect.com/science/article/pii/0370269373900476

[5] K.-H. Schmidt, J. Benlliure, A. Junghans, Fission of nuclei far from stability, Nucl. Phys. A 693 (1) (2001) 169–189. doi:https://doi.org/10.1016/S0375-9474(01)00648-0. URL https://www.sciencedirect.com/science/article/pii/S0375947401006480

[6] A. N. Andreyev, J. Elseviers, M. Huyse, P. Van Duppen, S. Antalic, A. Barzakh, N. Bree, T. E. Cocolios, V. F. Comas, J. Diriken, D. Fedorov, V. Fedosseev, S. Franchoo, J. A. Heredia, O. Ivanov, U. Köster, B. A. Marsh, K. Nishio, R. D. Page, N. Patronis, M. Seliverstov, I. Tsekhanovich, P. Van den Bergh, J. Van De Walle, M. Venhart, S. Vermote, M. Veselsky, C. Wagemans, T. Ichikawa, A. Iwamoto, P. Möller, A. J. Sierk, New type of asymmetric fission in proton-rich nuclei, Phys. Rev. Lett. 105 (2010) 252502. doi:10.1103/PhysRevLett.105.252502. URL https://link.aps.org/doi/10.1103/PhysRevLett.105.252502

[7] K. Nishio, A. Andreyev, R. Chapman, X. Derkx, C. Düllmann, L. Ghys, F. Heßberger, K. Hirose, H. Ikezoe, J. Khuyagbaatar, B. Kindler, B. Lommel, H. Makii, I. Nishinaka, T. Ohtsuki, S. Pain, R. Sagaidak, I. Tsekhanovich, M. Venhart, Y. Wakabayashi, S. Yan, Excitation energy dependence of fragment-mass distributions from fission of ^{180,190}Hg formed in fusion reactions of ^{36}Ar+ ^{144,154}Sm, Phys. Lett. B 748 (2015) 89–94. doi:https://doi.org/10.1016/j.physletb.2015.06.068. URL https://www.sciencedirect.com/science/article/pii/S0370269315004980

[8] E. M. Kozulin, G. N. Knyazheva, I. M. Itkis, M. G. Itkis, Y. S. Mukhamejanov, A. A. Bogachev, K. V. Novikov, V. V. Kirakosyan, D. Kumar, T. Banerjee, M. Cheralu, M. Maiti, R. Prajapat, R. Kumar, G. Sarkar, W. H. Trzaska, A. N. Andreyev, I. M. Harca, A. Mitu, E. Vardaci, Fission of ^{180,182,183}Hg* and ^{178}Pt* nuclei at intermediate excitation energies, Phys. Rev. C 105 (2022) 014607. doi:10.1103/PhysRevC.105.014607.
URL https://link.aps.org/doi/10.1103/PhysRevC.105.014607

[9] E. Prasad, D. Hinde, M. Dasgupta, D. Jeung, A. Berriman, B. Swinton-Bland, C. Simenel, E. Simpson, R. Bernard, E. Williams, K. Cook, D. Rafferty, C. Sengupta, J. Smith, K. Vo-Phuoc, J. Walshe, Systematics of the mass-asymmetric fission of excited nuclei from ^{176}Os to ^{206}Pb, Phys. Lett. B 811 (2020) 135941. doi:https://doi.org/10.1016/j.physletb.2020.135941.
URL https://www.sciencedirect.com/science/article/pii/S0370269320307449

[10] D. Kumar, E. Kozulin, M. Cheralu, G. Knyazheva, I. Itkis, M. Itkis, K. Novikov, A. Bogachev, N. Kozulina, I. Diatlov, et al., Study of mass-asymmetric fission of ^{180,190}Hg formed in the ^{36}Ar $+^{144,154}$ Sm reactions, Bull. Russ. Acad. Sci.: Phys. 84 (2020) 1001–1006. doi:10.3103/S1062873820080213.
URL https://doi.org/10.3103/S1062873820080213

[11] D. Kumar, E. Kozulin, G. Knyazheva, M. Maiti, I. Itkis, A. Bogachev, K. Novikov, M. Cheralu, T. Banerjee, I. Diatlov, et al., Investigation on competing fission modes in ^{178}Pt* produced by ^{36}Ar + ^{142}Nd reaction up to high excitation energies, Bull. Russ. Acad. Sci.: Phys. 85 (2021) 1479–1485. doi:10.3103/S1062873821120194.
URL https://doi.org/10.3103/S1062873821120194

[12] A. A. Bogachev, E. M. Kozulin, G. N. Knyazheva, I. M. Itkis, M. G. Itkis, K. V. Novikov, D. Kumar, T. Banerjee, I. N. Diatlov, M. Cheralu, V. V. Kirakosyan, Y. S. Mukhamejanov, A. N. Pan, I. V. Pchelintsev, R. S. Tikhomirov, I. V. Vorobiev, M. Maiti, R. Prajapat, R. Kumar, G. Sarkar, W. H. Trzaska, A. N. Andreyev, I. M. Harca, E. Vardaci, Asymmetric and symmetric fission of excited nuclei of ^{180,190}Hg and ^{184,192,202}Pb formed in the reactions with ^{36}Ar and ^{40,48}Ca ions, Phys. Rev. C 104 (2021) 024623. doi:10.1103/PhysRevC.104.024623.
URL https://link.aps.org/doi/10.1103/PhysRevC.104.024623

[13] I. Tsekhanovich, A. Andreyev, K. Nishio, D. Denis-Petit, K. Hirose, H. Makii, Z. Matheson, K. Morimoto, K. Morita, W. Nazarewicz, R. Orlandi, J. Sadhukhan, T. Tanaka, M. Vermeulen, M. Warda, Observation of the competing fission modes in ^{178}Pt, Phys. Lett. B 790 (2019) 583–588. doi:https://doi.org/10.1016/j.physletb.2019.02.006.
URL https://www.sciencedirect.com/science/article/pii/S0370269319300978

[14] Kavita, K. S. Golda, T. K. Ghosh, A. Jhingan, P. Sugathan, A. Chatterjee, B. R. Behera, A. Kumar, R. Kumar, N. Saneesh, M. Kumar, A. Yadav, C. Yadav, N. Kumar, A. Banerjee, A. Rani, S. K. Duggi, R. Dubey, K. Rani, S. Noor, J. Acharya, H. Singh, Fusion-fission dynamics of ^{188,190}Pt through fission fragment mass distribution measurements, Phys. Rev. C 100 (2019) 024626. doi:10.1103/PhysRevC.100.024626.
URL https://link.aps.org/doi/10.1103/PhysRevC.100.024626

[15] R. Tripathi, S. Sodaye, K. Sudarshan, B. K. Nayak, A. Jhingan, P. K. Pujari, K. Mahata, S. Santra, A. Saxena, E. T. Mirgule, R. G. Thomas, Fission fragment mass distributions in ^{35}Cl $+^{144,154}$ Sm reactions, Phys. Rev. C 92 (2015) 024610. doi:10.1103/PhysRevC.92.024610.
URL https://link.aps.org/doi/10.1103/PhysRevC.92.024610

[16] T. N. Nag, R. Tripathi, S. Patra, A. Mhatre, S. Santra, P. C. Rout, A. Kundu, D. Chattopadhyay, A. Pal, P. K. Pujari, Fission fragment mass distribution in the ^{32}S $+^{144}$ Sm reaction, Phys. Rev. C 103 (2021) 034612. doi:10.1103/PhysRevC.103.034612.
URL https://link.aps.org/doi/10.1103/PhysRevC.103.034612

[17] S. Gupta, K. Mahata, A. Shrivastava, K. Ramachandran, S. Pandit, P. Rout, V. Parkar, R. Tripathi, A. Kumar, B. Nayak, E. Mirgule, A. Saxena, S. Kailas, A. Jhingan, A. Nasirov, G. Yuldasheva, P. Nadtochy, C. Schmitt, Competing asymmetric fusion-fission and quasifission in neutron-deficient sub-lead nuclei, Phys. Lett. B 803 (2020) 135297. doi:https://doi.org/10.1016/j.physletb.2020.135297.
URL https://www.sciencedirect.com/science/article/pii/S0370269320301015

[18] B. Swinton-Bland, J. Buete, D. Hinde, M. Dasgupta, T. Tanaka, A. Berriman, D. Jeung, K. Banerjee, L. Bezzina, I. Carter, K. Cook, C. Sengupta, C. Simenel, E. Simpson, M. Stoyer, Multi-modal mass-asymmetric fission of ^{178}Pt from simultaneous mass-kinetic energy fitting, Phys. Lett. B 837 (2023) 137655. doi:https://doi.org/10.1016/j.physletb.2022.137655.
URL https://www.sciencedirect.com/science/article/pii/S0370269322007894

[19] E. Prasad, D. J. Hinde, K. Ramachandran, E. Williams, M. Dasgupta, I. P. Carter, K. J. Cook, D. Y. Jeung, D. H. Luong, S. McNeil, C. S. Palshetkar, D. C. Rafferty, C. Simenel, A. Wakhle, J. Khuyagbaatar, C. E. Düllmann, B. Lommel, B. Kindler, Observation of mass-asymmetric fission of mercury nuclei in heavy ion fusion, Phys. Rev. C 91 (2015) 064605. doi:10.1103/PhysRevC.91.064605.
URL https://link.aps.org/doi/10.1103/PhysRevC.91.064605

[20] C. J. Lin, R. du Rietz, D. J. Hinde, M. Dasgupta, R. G. Thomas, M. L. Brown, M. Evers, L. R. Gasques, M. D. Rodriguez, Systematic behavior of mass distributions in ^{48}Ti-induced fission at near-barrier energies, Phys. Rev. C 85 (2012) 014611. doi:10.1103/PhysRevC.85.014611.
URL https://link.aps.org/doi/10.1103/PhysRevC.85.014611

[21] R. Kumar, M. Maiti, A. Pal, S. Santra, P. Kaur, M. Sagwal, A. Singh, P. C. Rout, A. Baishya, R. Gandhi, T. Santhosh, Shell effect driven fission modes in fragment mass and total kinetic energy distribution of ^{192}Hg*, Phys. Rev. C 107 (2023) 034614. doi:10.1103/PhysRevC.107.034614.
URL https://link.aps.org/doi/10.1103/PhysRevC.107.034614

[22] P. Kaur, M. Maiti, R. Kumar, A. Singh, H. Sharma, Y. Arafat, N. Saneesh, A. Parihari, M. Kumar, K. S. Golda, A. Jhingan, P. Sugathan, Investigation of the mass distribution of the ^{28}Si $+^{158}$ Gd system: Role of shell effects, Phys. Rev. C 110 (2024) 034613. doi:10.1103/PhysRevC.110.034613.
URL https://link.aps.org/doi/10.1103/PhysRevC.

110.034613

[23] S. Dhuri, K. Mahata, A. Shrivastava, K. Ramachandran, S. K. Pandit, V. Kumar, V. V. Parkar, P. C. Rout, A. Kumar, A. Chavan, S. Kaur, T. Santhosh, Measurement of mass and total kinetic energy distributions for the $^{12}C + ^{175}$ Lu system, Phys. Rev. C 106 (2022) 014616. doi:10.1103/PhysRevC.106.014616. URL https://link.aps.org/doi/10.1103/PhysRevC.106.014616

[24] B. M. A. Swinton-Bland, M. A. Stoyer, A. C. Berriman, D. J. Hinde, C. Simenel, J. Buete, T. Tanaka, K. Banerjee, L. T. Bezzina, I. P. Carter, K. J. Cook, M. Dasgupta, D. Y. Jeung, C. Sengupta, E. C. Simpson, K. Vo-Phuoc, Mass-asymmetric fission of ^{205,207,209}Bi at energies close to the fission barrier using proton bombardment of ^{204,206,208}Pb, Phys. Rev. C 102 (2020) 054611. doi:10.1103/PhysRevC.102.054611. URL https://link.aps.org/doi/10.1103/PhysRevC.102.054611

[25] K.-H. Schmidt, B. Jurado, C. Amouroux, C. Schmitt, General description of fission observables: GEF model code, Nucl. Data Sheets 131 (2016) 107–221. doi:https://doi.org/10.1016/j.nds.2015.12.009. URL https://www.sciencedirect.com/science/article/pii/S0090375215000745

[26] U. Brosa, H.-H. Knitter, T.-s. Fan, J.-m. Hu, S.-l. Bao, Systematics of fission-channel probabilities, Phys. Rev. C 59 (1999) 767–775. doi:10.1103/PhysRevC.59.767. URL https://link.aps.org/doi/10.1103/PhysRevC.59.767